

# Expanding the scope of pycnen-picolinate lanthanide chelates to potential theranostic applications.

Gwladys Nizou,<sup>1</sup> Chiara Favaretto,<sup>2,3</sup> Francesca Borgna,<sup>2</sup> Pascal V. Grundler,<sup>2</sup> Nathalie Saffon-Merceron,<sup>4</sup> Carlos Platas-Iglesias,<sup>5</sup> Olivier Fougère,<sup>6</sup> Olivier Rousseaux,<sup>6</sup> Nicholas P. van der Meulen,<sup>2,7</sup> Cristina Müller,<sup>2,3</sup> Maryline Beyler,<sup>1,\*</sup> Raphael Tripier,<sup>1,\*</sup>

<sup>1</sup>Univ. Brest, UMR CNRS 6521 CEMCA, 6 avenue Le Gorgeu, CS93837, 29200 Brest, France

<sup>2</sup>Center for Radiopharmaceutical Sciences, Paul Scherrer Institute, Forschungsstrasse 111, 5232 Villigen-PSI, Switzerland

<sup>3</sup>Department of Chemistry and Applied Biosciences, ETH Zurich, 8093 Zurich, Switzerland

<sup>4</sup>Service commun Rayons X ICT-FR2599, Université Paul Sabatier, Bâtiment 2R1, 118 route de Narbonne, 31062 Toulouse, Cedex 09, France

<sup>5</sup>Departamento de Química, Facultade de Ciencias & Centro de Investigaciones Científicas Avanzadas (CICA), Universidade da Coruña, 15071 A Coruña, Spain

<sup>6</sup>Guerbet group, Centre de Recherche d'Aulnay-sous-Bois, BP 57400, 95943 Roissy CdG Cedex, France.

<sup>7</sup>Laboratory of Radiochemistry, Paul Scherrer Institute, Forschungsstrasse 111, 5232 Villigen-PSI, Switzerland

**KEYWORDS** Pycnen, picolinate, terbium, lutetium, <sup>177</sup>Lu, <sup>161</sup>Tb, radiotherapy, theranostic

---

**ABSTRACT:** A family of three picolinate pycnen based ligands, previously investigated for the complexation of Y<sup>3+</sup> and some lanthanide ions (Gd<sup>3+</sup>, Eu<sup>3+</sup>), was studied with <sup>161</sup>Tb and <sup>177</sup>Lu in view of potential radiotherapeutic applications. The set of six Tb<sup>3+</sup> and Lu<sup>3+</sup> complexes was synthesized and fully characterized. The coordination properties in the solid state and in solution were thoroughly studied. Potentiometric titrations, corroborated by Density Functional Theory (DFT) calculations, showed the very high stability constants of the Tb<sup>3+</sup> and Lu<sup>3+</sup> complexes, which are associated to remarkable kinetic inertness for up to 30 days in 1 M HCl. A complete radiolabeling study performed with both <sup>161</sup>Tb and <sup>177</sup>Lu radionuclides, including experiments with regard to the stability with and without scavengers and kinetic inertness using challenging agents, proved that the ligands could reasonably compete with the DOTA analogue. To conclude, the potential of using the same ligand for both radiotherapy and optical imaging was highlighted for the first time.

---

## Introduction

Cationic lanthanides (Ln<sup>3+</sup>) are of high relevance because of their magnetic and optical properties. For example, the symmetric <sup>8</sup>S ground state of Gd<sup>3+</sup> results in slow electron relaxation, which makes Gd<sup>3+</sup> complexes efficient contrast agents in magnetic resonance imaging (MRI).<sup>1</sup> Additionally almost all Ln<sup>3+</sup> ions (except La<sup>3+</sup> and Lu<sup>3+</sup>) are luminescent with characteristic emission wavelengths for each Ln<sup>3+</sup> (from UV to NIR).<sup>2</sup>

Some lanthanides, mainly Tb<sup>3+</sup>, Ho<sup>3+</sup> and Lu<sup>3+</sup>, have radioisotopes potentially suitable for the development of diagnostic and therapeutic radiopharmaceuticals in nuclear medicine.<sup>3,4</sup> For that purpose, the radiation properties of the therapeutic radionuclide should match the size/volume ratio of the targeted lesion to avoid affecting the surrounding healthy tissues.

The characteristics of β-emitting radionuclides of rare-earth elements are summarized in Table 1.

The radionuclide <sup>90</sup>Y has been widely used for therapeutic purposes thanks to its suitable decay properties. Meanwhile, <sup>90</sup>Y was mainly substituted by medium-energy β-emitters, such as <sup>177</sup>Lu, which is probably more appropriate for treating minimal residual disease.<sup>3</sup> The β-emission of <sup>177</sup>Lu is accompanied by several γ-photons with energies of 208 keV (10%) and 113 keV (6.2%), which are useful for SPECT imaging and, hence, dosimetry. <sup>161</sup>Tb, a potentially interesting β-emitter with similar properties to <sup>177</sup>Lu, co-emits conversion and Auger electrons. Its γ-radiation (75 keV, 10.2%) is useful for SPECT imaging.<sup>3</sup> There are other clinically interesting radioisotopes of terbium with complementary physical decay characteristics: <sup>149</sup>Tb (α-therapy), <sup>152</sup>Tb (PET) and <sup>155</sup>Tb (SPECT).

Table 1. Decay properties of  $\beta$ -emitting rare-earth elements for radiotherapy.<sup>5-8</sup>

Radioelement	$t_{1/2}$	$E_{\beta\text{mean}}$ (keV)	$E_{\gamma}$ (keV)	Max. range (mm)	Average range (mm)
<sup>90</sup> Y	64.0 h	934	-	11	2.5
<sup>166</sup> Ho	26.8 h	665	80.6 (6.6%)	8.7	2.2
<sup>161</sup> Tb	6.95 d	154	74.6 (10.2%)	-	0.15
<sup>177</sup> Lu	6.65 d	134	208.4 (10.4%)	2.2	0.67

Based on the growing interest for radiolanthanides in the field of nuclear medicine, the development of stable and inert  $\text{Ln}^{3+}$  chelates presenting fast radiolabeling under mild conditions is of great interest. The octadentate ligand DOTA (1,4,7,10-tetraazacyclododecane-1,4,7,10-tetraacetic acid) is probably the best known ligand for lanthanide(III) coordination,<sup>9</sup> despite slow complexation kinetics, and is successfully used (pre)clinically for radiolabeling with <sup>90</sup>Y, <sup>177</sup>Lu and <sup>161</sup>Tb.

However, to explore the luminescent properties of  $\text{Ln}^{3+}$  ions the DOTA scaffold is not well adapted, since it lacks a conjugated antenna essential to provoke the indirect excitation of the lanthanide(III) center through energy transfer processes. Additionally, DOTA- $\text{Ln}^{3+}$  complexes present an inner-sphere water molecule leading to non-radiative quenching by proximate O-H oscillators.<sup>10</sup>

Numerous chelators, often saturated azamacrocycles based on cyclen (1,4,7,10-tetraazacyclododecane),<sup>11</sup> tacn (1,4,7-triazacyclononane)<sup>12</sup> or even on cyclam (1,4,8,11-tetraazacyclotetradecane),<sup>13</sup> have been developed to form stable and/or inert lanthanide complexes for medical and bio-analytical applications. Pyclen (3,6,9,15-tetraazabicyclo[9.3.1]-pentadeca-1(15),11,13-triene), less investigated until recently, leads rapidly to the formation of remarkably inert  $\text{Ln}^{3+}$  complexes. For example, PCTA derivatives (3,6,9,15-tetraazabicyclo[9.3.1]pentadeca-1(15),11,13-triene-3,6,9-triacetic acid) are mainly explored for MRI due to its relatively high proton relaxivity.<sup>14, 15</sup>

We recently described the synthesis of the pyclen-based ligands **L1**, **L2**, **L3** and **L4**, and investigated their ability for  $\text{Y}^{3+}$  and  $\text{Ln}^{3+}$  coordination (Chart 1).<sup>16</sup> These four chelators, which are differentiated from each other by the relative position and number of acetate or picolinate functions, behave as octa- (**L1** and **L2**) or nonadentate (**L3** and **L4**) ligands upon coordination to the  $\text{Ln}^{3+}$  ions, leading to specific properties. If **L1** was presented as the least suited for  $\text{Ln}^{3+}$  coordination (presence of an acetate function in a labile apical position of the coordination sphere), it was demonstrated that **L2**, **L3** and **L4** present higher thermodynamic stabilities with  $\text{Gd}^{3+}$  and  $\text{Y}^{3+}$  at physiological pH than DOTA. **L4** stands out, in particular, for the higher kinetic inertness of its  $\text{Gd}^{3+}$  and  $\text{Y}^{3+}$  complexes, while the monohydrated **L2**- $\text{Gd}^{3+}$  complex can be considered as an interesting alternative to the DOTA analogue for MRI. The complexes of **L3** and **L4** show promise for optical imaging, thanks to their high emission quantum yields ( $\Phi$ ) and long luminescence lifetimes ( $\tau_{\text{H}_2\text{O}}$ ) in aqueous medium, especially for  $\text{Tb}^{3+}$  ( $\Phi > 95\%$ ;  $\tau_{\text{H}_2\text{O}} \sim 2.5$  ms).<sup>16(d)</sup>

Taking these encouraging results into consideration, it was hypothesized that **L2**, **L3** and **L4** may have potential as chelators for several radionuclides, including <sup>177</sup>Lu and <sup>161</sup>Tb.

Moreover, <sup>161</sup>Tb radiocomplexes formed with **L3** and **L4** may also be useful as potential theranostic agents, since the luminescence properties of  $\text{Tb}^{3+}$  can be exploited for optical imaging. A detailed study of the  $\text{Lu}^{3+}$  and  $\text{Tb}^{3+}$  complexes with **L2**-**L4** in solution and in the solid state is reported. Radiolabeling studies with <sup>177</sup>Lu and <sup>161</sup>Tb were then performed and the stability of the corresponding complexes investigated in various media.

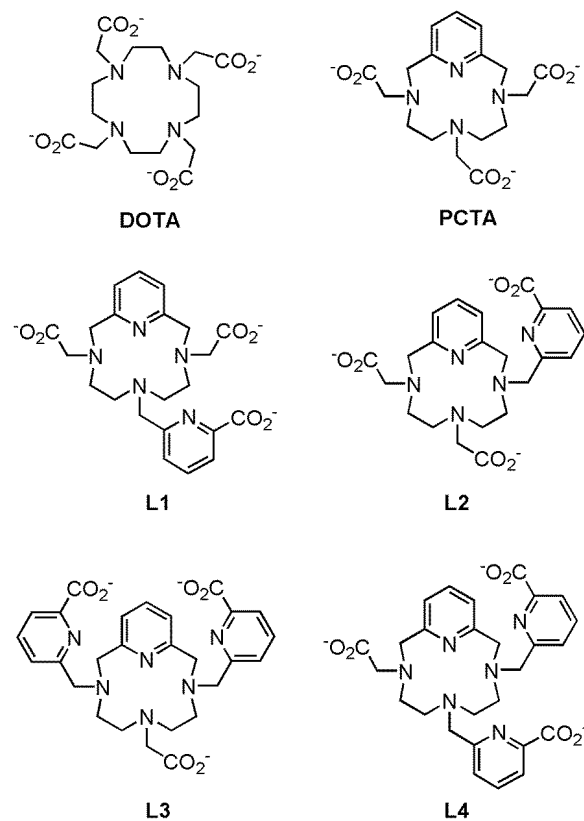


Chart 1. Chemical structures of DOTA, PCTA as well as L1-L4.

## Results and Discussion

### Ligand synthesis and complexation with $\text{Tb}^{3+}$ and $\text{Lu}^{3+}$

The **L2**, **L3** and **L4** ligands were synthesized as described previously,<sup>16(a-b)</sup> but some steps have been optimized in order

to improve the overall yields. The adapted/optimized procedures are described and discussed in the Supporting Information SI (Schemes S1-S3; Figures S1-S4).

The corresponding LnL2, LnL3 and LnL4 complexes (Ln = Tb and Lu) were prepared by reaction of the ligands with LnCl<sub>3</sub>·6H<sub>2</sub>O in aqueous solution at pH 5, isolated with quantitative yields by precipitation in methanol and characterized by high-resolution mass spectroscopy (ESI<sup>+</sup> ionization) (Figures S5-S10, Supporting Information).

The diamagnetic Lu<sup>3+</sup> complexes could be characterized by <sup>1</sup>H and <sup>13</sup>C NMR. The spectra are given in Supporting Information (Figures S11-S16). The <sup>1</sup>H spectra show very sharp peaks, indicating the formation of well-defined rigid species.

Both <sup>1</sup>H and <sup>13</sup>C spectra show a single set of signals corresponding to the formation of complexes with a 1:1 (Lu:L) stoichiometry.

### X-ray crystal structures

Slow evaporation of methanolic solutions of LnL3 and LnL4 (Ln = Tb or Lu) provided single crystals suitable for X-ray diffraction analyses. The structures of the four complexes and their corresponding coordination polyhedra are shown in Figures 1 and 2, while Table 2 and Table 3 present the bond distances of the coordination spheres of the metal ions for LnL3 and LnL4, respectively. All the crystallographic data are given in Table S1 in Supporting Information.

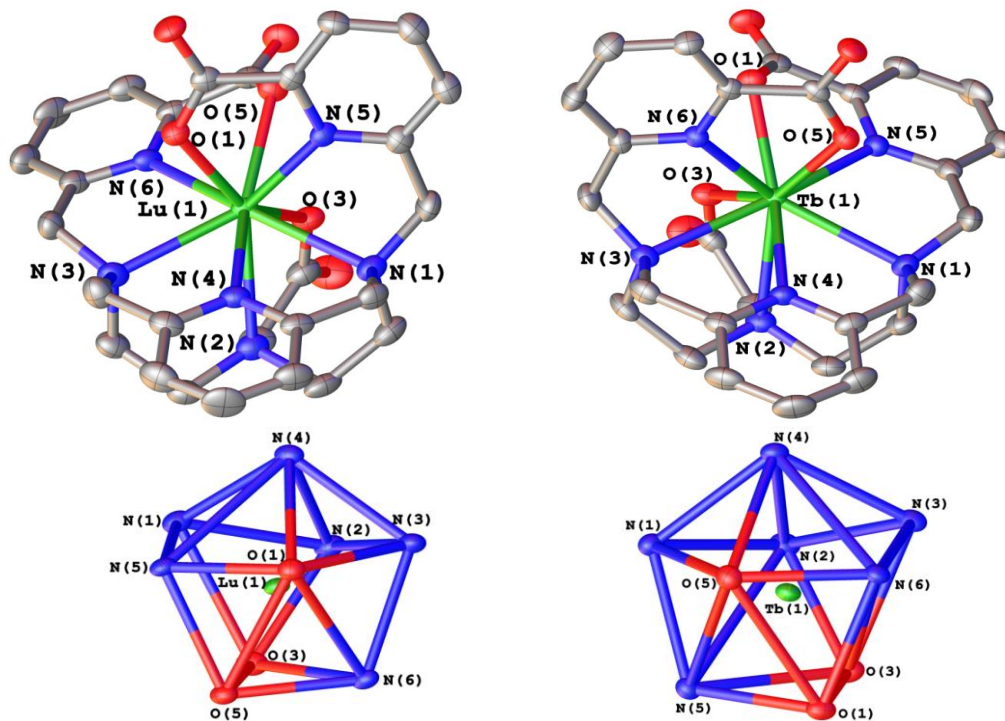


**Figure 1.** View of the crystal structures of LuL3 and TbL3 (top) and the corresponding coordination polyhedra around the metal ions (bottom). Hydrogen atoms and water molecules are omitted for clarity. The ORTEP plot is at the 50% probability level.

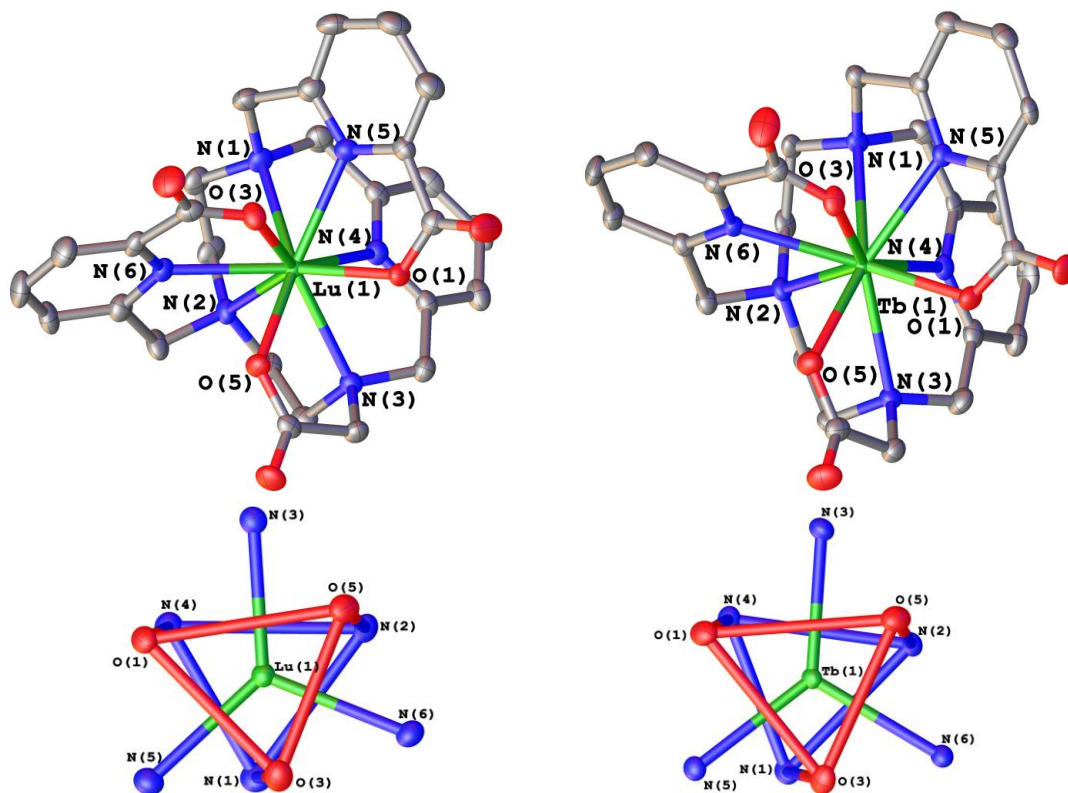


**Figure 2.** View of the crystal structures of LuL4 and TbL4 (top) and the corresponding coordination polyhedra around the metal ions (bottom). Hydrogen atoms and water molecules are omitted for clarity. The ORTEP plot is at the 50% probability level.

X-ray diffraction of single crystals of LuL3 and TbL3 revealed that both compounds were isostructural and crystallized in the monoclinic  $C2/c$  space group (Table 2), with similar unit cell parameters. The two chelates are surrounded by 5.5 water molecules, one of them situated at a special position. LuL4 and TbL4 crystallized in the  $P2_1/n$  space group (Table 3), but their asymmetric units were different. The asymmetric unit of LuL4 contains three water molecules and another that was squeezed to properly resolve the structure.<sup>17</sup> However, TbL4 crystallized with the two enantiomers in the asymmetric unit and 13 water molecules. The crystal structures of LuL3, TbL3, LuL4 and TbL4 are very similar to those reported in previous works for the  $Yb^{3+}$ ,  $Eu^{3+}$  and  $Y^{3+}$  analogues.<sup>16(b),(a)</sup> The metal ion is directly coordinated to six nitrogen atoms and three oxygen atoms of pyclen and its picolinate and acetate arms. As discussed previously,<sup>16(a),(b)</sup> for LuL3 and TbL3 this results in a nine-fold coordination around the metal ion with a very distorted and irregular 1:5:3 coordination polyhedron containing three vertexes related by a 2-fold pseudosymmetry axis (O(5), O(3) and N(6), Figure 1), five vertexes related by a 5-fold pseudosymmetry axis (N(1), N(2), N(3), O(1) and N(5)) and the remaining vertex (N(4)) sitting on the latter axis.<sup>18</sup>

The coordination polyhedron in LuL4 and TbL4 can be also described by a similar 1:5:3 polyhedron, but also as a severely distorted tricapped trigonal prism (Figure 2), where the upper triangular face is defined by O(1), O(3) and O(5), and the lower triangular face is described by N(1), N(2) and N(4). These two planes intersect at  $11.8^\circ$  (LuL4),  $8.9^\circ$  and  $10.6^\circ$

(TbL4), reflecting rather distorted polyhedra. The upper and lower planes are not completely eclipsed, with twist angles of  $12.8^\circ$  (and  $18.3^\circ$ ) and  $16.8^\circ$  for LuL4 and TbL4, respectively.

The macrocyclic pyclen unit adopts a [4242] conformation in all complexes,<sup>19</sup> as already observed for  $Yb^{3+}$ ,  $Eu^{3+}$  and  $Y^{3+}$  derivatives.<sup>11(b),(d)</sup> Indeed, unlike cyclen derivatives that adopt a square [3333] conformation, the pyridine moiety of pyclen dictates that one side of the macrocycle must incorporate four bonds and so a [3333] conformation is impossible.<sup>20</sup> As a result, the four five-membered chelate rings formed by the coordination of the pyclen moiety adopt a  $(\delta\lambda\delta\lambda)$  conformation, which is characterized by the presence of a mirror plane that makes pyclen achiral.<sup>20</sup> Thus, the only source of chirality in these complexes was related to the layout of the pendant arms, which generate two enantiomers that can be denoted as  $\Delta$  and  $\Lambda$ .<sup>21</sup> As observed previously,<sup>16(b),(d)</sup> the two enantiomers are present in the crystal lattice related by an inversion center.

**Table 2. Bond distances ( $\text{\AA}$ ) to metal center for LnL3 structures (Ln = Eu, Tb, Y, Yb and Lu).**

	EuL3 <sup>a</sup>	TbL3	YL3 <sup>b</sup>	YbL3 <sup>a</sup>	LuL3
Ln <sup>3+</sup> ionic radius ( $\text{\AA}$ ) CN=9 <sup>c</sup>	1.12	1.095	1.075	1.042	1.032
Ln(1)-N(1)	2.868	2.624	2.606	2.596	2.557

Ln(1)-N(2)	2.703	2.641	2.630	2.629	2.606
Ln(1)-N(3)	2.676	2.599	2.614	2.593	2.591
Ln(1)-N(4)	2.625	2.542	2.486	2.459	2.484
Ln(1)-N(5)	2.615	2.478	2.458	2.437	2.379
Ln(1)-N(6)	2.594	2.439	2.476	2.459	2.426
Ln(1)-O(1)	2.467	2.390	2.327	2.311	2.310
Ln(1)-O(3)	2.513	2.364	2.315	2.304	2.303
Ln(1)-O(5)	2.415	2.374	2.398	2.392	2.363
Ln(1)-O(3) <sup>c</sup>	2.453	-	-	-	-

<sup>a</sup>From ref. (16(d)); <sup>b</sup>From ref. (16(b)); <sup>c</sup>From ref. (22)

The bond distances of the metal coordination environments generally decrease along the lanthanide series as a result of the lanthanide contraction,<sup>23</sup> with the exception of the Ln(1)-N(4) distance, which is slightly longer for LuL3 than YbL3 (Table 2), and the Ln(1)-N(1) and Ln(1)-N(5) distances, which are longer for LuL4 than YbL4 (Table 3). This suggests that the coordination of the nine donor atoms of the ligand is sterically more demanding for the smallest lanthanide ions.

**Table 3. Bond distances (Å) to metal center for LnL4 structures (Ln = Eu, Tb, Y, Yb and Lu).**

	EuL4 <sup>a</sup>	TbL4 <sup>b</sup>	YL4 <sup>c</sup>	YbL4 <sup>a</sup>	LuL4
Ln <sup>3+</sup> ionic radius (Å) CN=9 <sup>d</sup>	1.12	1.095	1.075	1.042	1.032
Ln(1)-N(1)	2.648	2.637-2.624	2.603	2.604	2.610
Ln(1)-N(2)	2.647	2.621-2.659	2.645	2.591	2.568
Ln(1)-N(3)	2.592	2.571-2.583	2.575	2.538	2.526
Ln(1)-N(4)	2.600	2.571-2.571	2.548	2.515	2.465
Ln(1)-N(5)	2.501	2.475-2.480	2.465	2.453	2.470
Ln(1)-N(6)	2.558	2.529-2.553	2.535	2.483	2.462
Ln(1)-O(1)	2.358	2.326-2.335	2.307	2.272	2.264
Ln(1)-O(3)	2.419	2.402-2.386	2.361	2.359	2.330
Ln(1)-O(5)	2.375	2.353-2.359	2.338	2.304	2.287

<sup>a</sup>From ref. (16(d)); <sup>b</sup>Data of the two enantiomers present in the asymmetric unit.; <sup>c</sup>From ref. (16(b)); <sup>d</sup>From ref. (22)

### Kinetics

Because of lanthanide contraction,<sup>23,24</sup> an increasing kinetic inertness is expected across the lanthanide series as a result of the stronger electrostatic interaction between the ligand and the metal ion, associated to the enhanced positive charge density of the latter. The dissociation kinetics of all the Lu<sup>3+</sup> and Tb<sup>3+</sup> complexes were studied in 1.0 M HCl by UV-Vis spectroscopy, following the change of absorbance due to the  $\pi$ - $\pi^*$  transition band of the aromatic units (Supporting Information, Figure S17-S22). As presented in Table 4, dissociation half-lives ( $t_{1/2}$ ) globally increase from Tb<sup>3+</sup> complexes to Lu<sup>3+</sup> ones, following the lanthanide contraction, as expected.

**Table 4. Dissociation half-lives ( $t_{1/2}$ ) in min of LnL complexes in 1 M HCl (Ln = Tb or Lu, L= L2, L3 or L4) and comparison with the Y<sup>3+</sup> analogues.**

	L2	L3	L4
Y <sup>a</sup>	357	140	41880
Tb	178	296	22602
Lu	671	785	> 30 days

<sup>a</sup>From ref. (16(a),(b))

The acid-assisted dissociation was proven to be one order of magnitude faster for Ln(PCTA) complexes than for the Ln(DOTA)<sup>-</sup> analogues.<sup>14</sup> However, as already shown with Y<sup>3+</sup>, the substitution of acetate arms with picolinate groups considerably increases the kinetic inertness of the complexes, reaching or even surpassing those of Ln(DOTA)<sup>-</sup> chelates.<sup>16(a),(b)</sup>

An interesting feature of the complexes investigated here is that the LnL4 complexes are considerably more inert than their LnL3 counterparts. The dissociation of these complexes under strongly acidic conditions follows the acid-catalyzed mechanism, with the formation of a protonated intermediate. Complex protonation facilitates partial decoordination of the ligand, which triggers complex dissociation. The bond distances of the metal coordination environment reported in Table 2 and Table 3 show that the LuL3 complex presents a particularly long Lu-O(5) distance (2.363 Å), which would explain the faster dissociation kinetics compared with LuL4, for which Lu-O distances range from 2.26 to 2.33 Å. However, the longer Ln-O distance among the Tb<sup>3+</sup> complex is observed for the more inert TbL4 complex. Thus, we hypothesize that the different kinetic inertness of LnL3 and LnL4 complexes is likely related to their different ability to protonate associated to distinct charge distributions.

### DFT calculations

**Table 5. Protonation constants of the picolinate pyclen-based ligands and stability constants of the corresponding LnL complexes (Ln = Tb, Lu, L = L2-L4) and comparison with ligands of reference at 25°C.**

	L2	L3	L4	PCTA	DOTA
log $K_1^H$	11.30(1) <sup>a</sup>	11.30(2) <sup>a</sup>	10.50(2) <sup>a</sup>	11.36 <sup>e</sup>	12.09 <sup>g</sup>
log $K_2^H$	6.46(1) <sup>a</sup>	5.58(2) <sup>a</sup>	6.73(3) <sup>a</sup>	7.35 <sup>e</sup>	9.68 <sup>g</sup>
log $K_3^H$	4.27(1) <sup>a</sup>	4.23(2) <sup>a</sup>	3.86(3) <sup>a</sup>	3.83 <sup>e</sup>	4.55 <sup>g</sup>
log $K_4^H$	2.90(1) <sup>a</sup>	3.01(2) <sup>a</sup>	2.98(2) <sup>a</sup>	2.12 <sup>e</sup>	4.13 <sup>g</sup>
log $K_5^H$	-	-	-	1.29 <sup>e</sup>	-
log $K_{GdL}$	22.37(3) <sup>b</sup>	23.56(2) <sup>c</sup>	23.44(2) <sup>c</sup>	20.39 <sup>e</sup>	24.67 <sup>h</sup>
log $K_{YL}$	22.44(2) <sup>b</sup>	23.36(2) <sup>b</sup>	23.07(2) <sup>d</sup>	20.28 <sup>e</sup>	24.9 <sup>i</sup>
log $K_{TbL}$	21.4(1) <sup>a</sup>	23.8(4) <sup>a</sup>	25.2(1) <sup>a</sup>	20.39 <sup>f</sup>	24.22 <sup>h</sup>
log $K_{LuL}$	24.32(6) <sup>a</sup>	25.9(6) <sup>a</sup>	27.1(2) <sup>a</sup>	n.f.	25.41 <sup>h</sup>
pGd <sup>j</sup>	20.3	20.7	21.8	17.0	19.2
pY <sup>j</sup>	20.3	20.5	21.5	17.0	18.9
pTb <sup>j</sup>	17.6	20.4	22.6	16.2	17.2
pLu <sup>j</sup>	20.5	22.4	24.5	n.f.	18.4

<sup>a</sup>this work (I = 0.1 M KNO<sub>3</sub>), <sup>b</sup>ref. (16(a)) (I = 0.15 M NaCl), <sup>c</sup>ref. (16(c)) (I = 0.15 M NaCl), <sup>d</sup>ref. (16(a)) (I = 0.15 M NaCl), <sup>e</sup>ref. (14) (I = 1.0 M KCl), <sup>f</sup>ref. (25) (I = 0.1 M KCl). <sup>g</sup>ref. (26) (I = 0.15 M Me<sub>4</sub>NNO<sub>3</sub>), <sup>h</sup>ref. (9(b)) (I = 0.1 M NaCl), <sup>i</sup>ref. (27) (I = 0.1 M Me<sub>4</sub>NNO<sub>3</sub>), <sup>j</sup> values calculated for 100% excess of ligand with [M]<sub>tot</sub> = 1.0 × 10<sup>-5</sup> M, at pH 7.4, with the given protonation and stability constants; n.f.: not available in the literature to our knowledge.

To find support for this hypothesis, we modeled the LnL3 and LnL4 complexes using DFT calculations (see computational details below, Table S2), and calculated the electrostatic potential on the molecular surface of the complex defined by an isodensity value of 0.0004 electrons Bohr<sup>-3</sup>.<sup>24</sup> The results show that the surfaces of the two complexes present a hydrophobic region on the backside of pyclen fragment and a second region characterized by a negative electrostatic potential on the side of the molecule where the pendant arms are situated. Our calculations predict a very different distribution of the electrostatic potential on the molecular surface (Figure 3). In the case of LuL4, the tricapped trigonal prismatic coordination places the oxygen atoms of the carboxylate groups in the same region. Complex protonation is expected to occur at oxygen atoms of carboxylate groups that are not coordinated to the metal ion, which in LuL4 are pointing outwards (Table S3). These oxygen atoms hold a significant negative electrostatic potential, but are quite apart from each other (O...O distances > 6.0 Å). In LuL3 two uncoordinated oxygen atoms in the periphery of the complex hold significant negative electrostatic potential, and are placed at a relatively short distance of 4.75 Å (Table S4). These results suggest that the LnL3 complexes may be more prone to protonate due to the presence of a higher negative charge density, which likely facilitates the decoordination of one of the pendant arms, triggering complex dissociation.

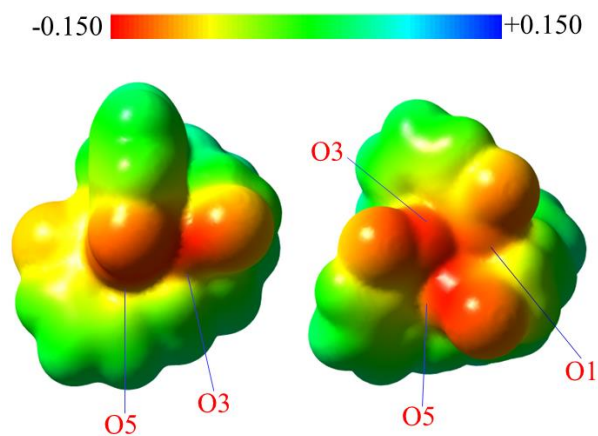


**Figure 3.** Views of the electrostatic potential on a 0.0004 electrons Bohr<sup>-3</sup> isosurface of the electron density, obtained with DFT calculations, for LuL3 (left) and LuL4 (right).

#### Thermodynamic stability

Because of the complete complexation in acidic pH, stability constant values of L2, L3 and L4 for M = Tb and Lu could not be determined by conventional potentiometric experiments, but only by competition with DOTA using the out-of-cell method with KNO<sub>3</sub> as electrolyte (I = 0.1 M). The protonation constants of the three ligands, already measured in NaCl (I = 0.15M),<sup>16(a),(b)</sup> were measured again in the conditions used for the determination of the stability constants (Table 5). The out-of-cell competition method used solutions containing L:M:DOTA (1:1:1) at different pH values, incubated at 25°C and measured after four weeks (until no more change of potential occurred).

The log  $K_{ML}$  values for  $M = Tb$  and  $Lu$ , as well as the stability constants of the complexes with  $Y^{3+}$  and  $Gd^{3+}$  reported in our previous work,<sup>16</sup> are listed in Table 5. For comparison, literature data of DOTA and PCTA with the same metals are also reported. The  $Lu^{3+}$  complexation constant with PCTA was not found in the literature, despite that this ligand was already employed for  $^{177}Lu$  radiolabeling, *vide infra*.<sup>28</sup>

The stability constants obtained for the three lanthanide ions ( $Gd^{3+}$ ,  $Tb^{3+}$  and  $Lu^{3+}$ ) with picolinate cyclen-based chelators follow the same trend as that reported for DOTA by Sherry *et al.*<sup>9(b)</sup>  $Gd^{3+}$  and  $Tb^{3+}$  complexes are characterized by similar thermodynamic stabilities, whereas the  $Lu^{3+}$  analogues show higher stability constants. Most lanthanide ions form complexes with stabilities that increase across the lanthanide series, as a result of the increased charge density of the metal ion. In a few cases, stability constants reach a maximum at a certain point of the series and then decrease, or even decrease steadily along the series. In these situations, ligand rigidity and/or steric effects are responsible for the decreased stability as the ionic radius of the metal ion decreases.<sup>29</sup> Thus, we conclude

that the coordination of **L2**, **L3** and **L4** does not introduce significant steric hindrance to the small lanthanide ions. The experiments performed in this work strongly confirmed the previous calculations that predict, for instance, that  $LuL4$  should be more stable than  $LuL3$  by 1.5 log $K$  units, which is in good agreement with the potentiometric data and validates our investigation approach. The speciation diagrams drawn from the protonation and stability constants show no free  $Ln^{3+}$  metal over the whole pH range (2-11).  $LnL$  was the predomi-

nant species under the chosen radiolabeling conditions (pH 5) and was the only species present at the physiological pH of 7.4 (Figure S23-S25). The values obtained for both  $Tb^{3+}$  and  $Lu^{3+}$  complexes of the cyclen-containing picolinate ligands are in the same order of magnitude than those for the DOTA analogues, proving the high thermodynamic stability of the  $LnL$  ( $L = L2, L3, L4$ ) chelates. A more relevant comparison of stability constants of complexes formed with ligands of different basicity is provided by the so-called pM values (pM is defined as  $-\log[M]_{free}$  and takes into account the competition between protonation and complexation for a given ligand at a given pH, in this case 7.4). The calculated values are tabulated in Table 5. Once again, pTb and pLu are largely higher for the picolinate-cyclen family of complexes as compared to PCTA and DOTA, making **L2-L4** polyvalent chelators with great potential to be used, as their Ln(III) chelates, for *in vivo* applications.

#### Radiolabeling and experiments with $^{161}Tb$ and $^{177}Lu$

The chelators **L2**, **L3** and **L4** were radiolabeled with  $^{161}Tb$ , as well as the clinically-employed  $^{177}Lu$ . The stability of the resultant radiometal complexes was compared to those of their

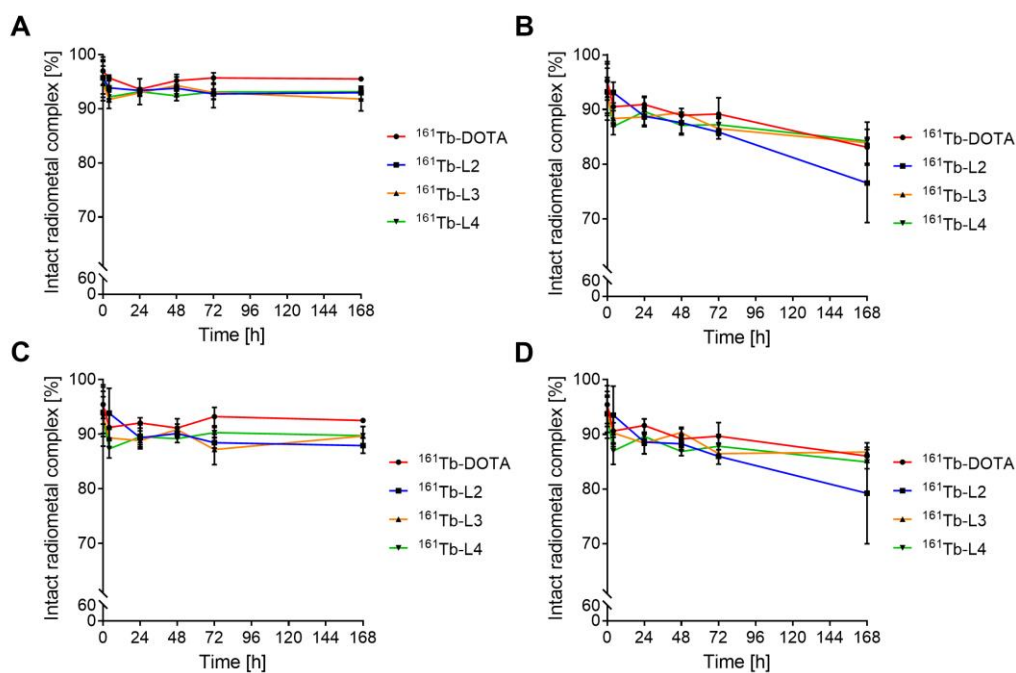


**Figure 4.** Graphs presenting the percentage of intact  $^{161}TbL$  ( $L = L2, L3$  or  $L4$ ) and  $^{161}Tb(DOTA)^-$  at room temperature. Incubation of the radiometal complexes in (a) saline and ethanol (pH = 5), (b) saline and ascorbic acid (pH = 4), (c) PBS and ethanol (pH = 7.4) and (d) PBS and ascorbic acid (pH = 7.4). For some of the data points, the standard deviation were small and, hence, not visible.

that the coordination of **L2**, **L3** and **L4** does not introduce significant steric hindrance to the small lanthanide ions. The experiments performed in this work strongly confirmed the previous calculations that predict, for instance, that  $LuL4$  should be more stable than  $LuL3$  by 1.5 log $K$  units, which is in good agreement with the potentiometric data and validates our investigation approach. The speciation diagrams drawn from the protonation and stability constants show no free  $Ln^{3+}$  metal over the whole pH range (2-11).  $LnL$  was the predomi-

nant species under the chosen radiolabeling conditions (pH 5) and was the only species present at the physiological pH of 7.4 (Figure S23-S25). The values obtained for both  $Tb^{3+}$  and  $Lu^{3+}$  complexes of the cyclen-containing picolinate ligands are in the same order of magnitude than those for the DOTA analogues, proving the high thermodynamic stability of the  $LnL$  ( $L = L2, L3, L4$ ) chelates. A more relevant comparison of stability constants of complexes formed with ligands of different basicity is provided by the so-called pM values (pM is defined as  $-\log[M]_{free}$  and takes into account the competition between protonation and complexation for a given ligand at a given pH, in this case 7.4). The calculated values are tabulated in Table 5. Once again, pTb and pLu are largely higher for the picolinate-cyclen family of complexes as compared to PCTA and DOTA, making **L2-L4** polyvalent chelators with great potential to be used, as their Ln(III) chelates, for *in vivo* applications.

#### Stability of radiometal complexes

Radiolysis was observed over a four-day period for all terbium radiometal complexes, such as  $^{161}\text{TbL}$  ( $\text{L} = \text{L2, L3}$  or  $\text{L4}$ ), as well as for  $^{161}\text{Tb}(\text{DOTA})^-$  when diluted in Milli-Q water, saline or PBS without scavengers (SI, Figure S26). At most, 30% of intact  $^{161}\text{TbL}$  complex remained after four days' incubation in these solutions at room temperature. Signs of radiolysis were already obvious after 24 hours, when the content of intact product decreased to <70%. The same behavior was observed for  $^{161}\text{Tb}(\text{DOTA})^-$ . In order to demonstrate that the degradation of the radiometal complexes was related to the activity,  $^{161}\text{TbL2}$  was prepared at a lower molar activity (5 MBq/nmol). Under these conditions, in which the ligands were

and  $^{161}\text{Tb}(\text{DOTA})^-$  showed on average  $93 \pm 2\%$  intact product in saline in the presence of ethanol, but only  $82 \pm 4\%$  when ascorbic acid was added to the saline. It is possible that ascorbic acid was lost by aerobic oxidation over time, hence, a better effect may also be achieved with increased concentrations of ascorbic acid.

In conclusion, the use of ethanol and saline improved the stability of the  $^{161}\text{Tb}$ -radiometal complexes most favorably. Similar results were also observed for the  $^{177}\text{Lu}$ -complexes (Figure S28).

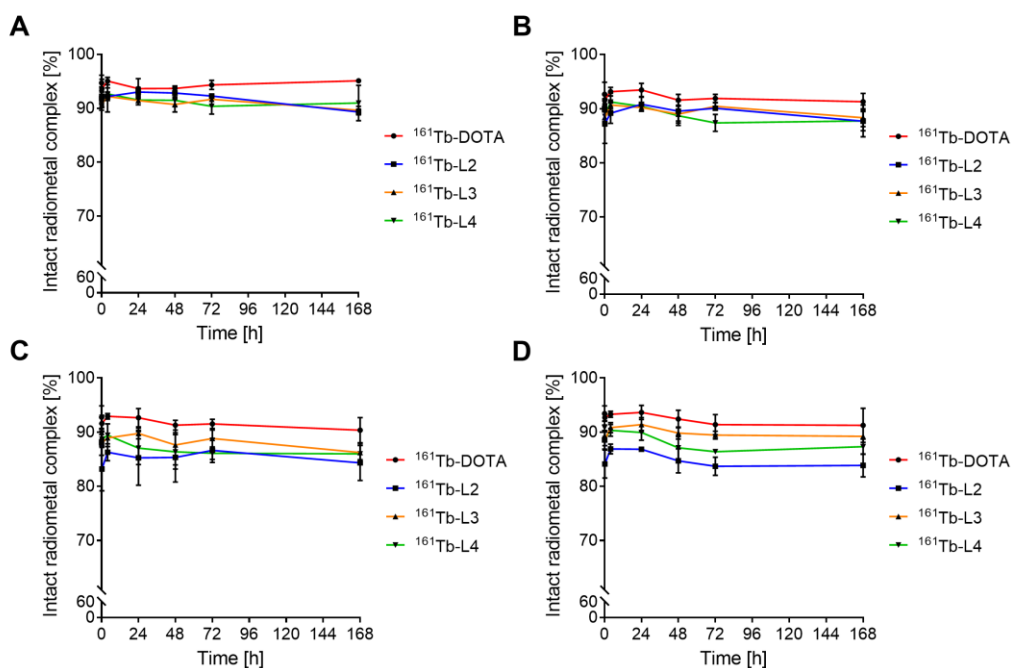


**Figure 5.** Graphs presenting the percentage of intact  $^{161}\text{TbL}$  ( $\text{L} = \text{L2, L3}$  or  $\text{L4}$ ) and  $^{161}\text{Tb}(\text{DOTA})^-$  over time. Incubation of the radiometal complexes with a 1000-fold excess of (a) DTPA, (b) EDTA, (c) Fe(II) and (d) Zn(II), in saline-ethanol solution (pH=5). For some of the points, the standard deviation bars are shorter than the height of the symbol, making them impossible to visualize.

present in 10-fold higher excess, the stability of the radiometal complexes was increased (SI, Figure S27). After four days,  $64 \pm 2\%$ ,  $63 \pm 1\%$  and  $62 \pm 1\%$  of  $^{161}\text{TbL2}$  were intact in MilliQ-water, saline and PBS, respectively.

In an attempt to stabilize the  $^{161}\text{Tb}$ - and  $^{177}\text{Lu}$ -complexes, radical scavengers, such as ethanol or ascorbic acid, were added to the incubation solution. The effect of both agents on the stability of the radiometal complexes was investigated using saline or PBS (Figure 4), respectively. The three  $^{161}\text{TbL}$  complexes, as well as  $^{161}\text{Tb}(\text{DOTA})^-$  showed improved stability (>85%) in the presence of scavengers for both saline and PBS at room temperature over the first 24 hours. Over more extended periods, ethanol was found to stabilize the radiometal complexes better than ascorbic acid, particularly in saline solution. Indeed, after seven days the three  $^{161}\text{TbL}$  complexes

#### Kinetic inertness with challenging agents

High kinetic inertness of a radiometal complex is required to avoid any release of radiometal cation, which may accumulate at undesired sites when used *in vivo*. Release of the radiometal from the chelator may occur as a result of the dissociation of the complex outside the human body during the preparation of the radiopharmaceutical and/or after administration *in vivo*.<sup>30</sup> To ensure that the radiometal complexes evaluated in this study had comparable kinetic inertness to that of the clinically-used DOTA, transchelation and transmetallation processes were evaluated in the presence of excess chelating agents potentially present in the pharmaceutical formulation, DTPA or EDTA, and of common biological metal ions,  $\text{Zn}^{2+}$  or  $\text{Fe}^{2+}$ , respectively.

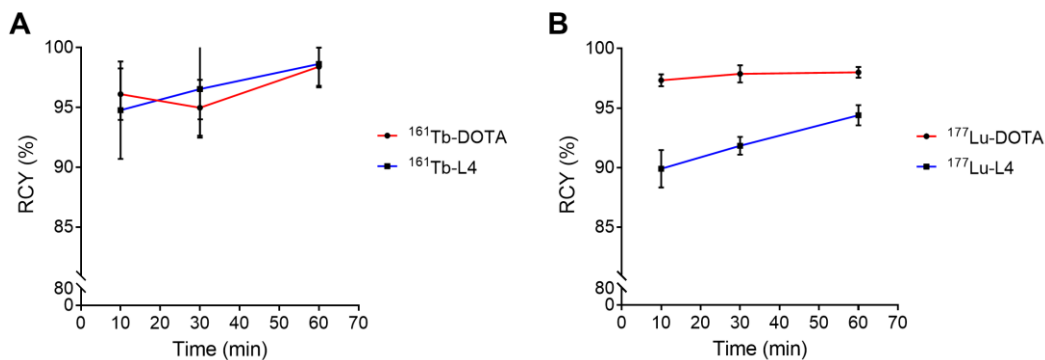


**Figure 6.** Graphs representing the amount of formed radiometal complex (RCY) of (a)  $^{161}\text{Tb-L4}$  and  $^{161}\text{Tb(DOTA)}^-$  and (b)  $^{177}\text{Lu-L4}$  and  $^{177}\text{Lu(DOTA)}^-$ , as a function of incubation time at 37 °C. For some of the points, the standard deviation bars are shorter than the height of the symbol, making them impossible to visualize.

Challenging experiments were carried out using a 1000-fold molar excess of chelator (DTPA or EDTA) or metallic ion ( $\text{Fe}^{2+}$  or  $\text{Zn}^{2+}$ ) in saline containing 10% ethanol as a scavenger. This large excess of metal complexation agents was used to provide a highly challenging environment, similar to the conditions used in previous studies.<sup>16(b),30</sup>  $^{161}\text{Tb(DOTA)}^-$  showed slightly higher stability compared to the  $^{161}\text{TbL}$  complexes. Under the given conditions, >80% intact radiometal complex was observed for up to seven days, which demonstrated relatively high inertness. To some degree, the radiometal complexes were more prone to transmetallation than to transchelation. The least stable radiometal complex in this regard was  $^{161}\text{TbL2}$ . Nevertheless,  $84 \pm 3\%$  and  $84 \pm 2\%$  of intact radiometal complex were determined after seven days in the presence of  $\text{Fe}^{3+}$  and  $\text{Zn}^{2+}$ , respectively (Figure 5).

Similar findings were observed with the  $^{177}\text{Lu}$ -complexes, which showed >80% intact product for up to seven days, under similar conditions to those also studied for the  $^{161}\text{Tb}$ -labeled complexes (SI, Figure S29).

#### Determination of radiolabeling kinetics at 37 °C

Throughout this study, the  $\text{LnL4}$  complexes showed the most promising characteristics in terms of thermodynamic stability and kinetic inertness, as it was demonstrated in the potentiometric and dissociation experiments. This ligand was, therefore, chosen and compared to DOTA for the investigation of the radiolabeling efficiency with  $^{161}\text{Tb}$  and  $^{177}\text{Lu}$  at the lower incubation temperature of 37 °C. The possibility of radiolabeling at lower temperatures would be ideal if such chelators were used for the modification of monoclonal antibodies, which are temperature sensitive due to protein denaturation at elevated temperatures. The radiolabeling yield (RCY), corresponding to the amount of radiometal complex formed, was evaluated at various incubation times at 37 °C. After 10 minutes of incubation of the radiolabeling mixture, the RCY of the radiometal complexes of **L4** and DOTA was already >90%. At this time point,  $^{161}\text{TbL4}$  and  $^{161}\text{Tb(DOTA)}^-$  were produced with similar radiolabeling yields, resulting in  $95 \pm 4\%$  and  $96 \pm 2\%$ , respectively. After 1 hour, the RCYs were >98% for  $^{161}\text{TbL4}$  and  $^{161}\text{Tb(DOTA)}^-$  (Figure 6 (a)). The radiolabeling of **L4** with  $^{177}\text{Lu}$  revealed a RCY of  $94 \pm 1\%$  after 1 hour. The radiolabeling of DOTA with  $^{177}\text{Lu}$  was even higher, at  $97 \pm 1\%$  after 10 minutes of incubation (Figure 6 (b)).

#### Evaluation of $\text{TbL4}$ emission

In a previous work, the luminescent properties of dipicolinate-pyclen  $\text{Tb}^{3+}$  complexes were highlighted.<sup>16(d)</sup> In the present work, a preliminary experiment of  $^{161}\text{Tb}^{3+}$  radiometal complex emission under UV light was performed.

The sensitivity of luminescent  $\text{Ln}^{3+}$  complexes is in the order of  $10^{-5}$  M. This could be confirmed by the absence of luminescence of the solution of  $^{161}\text{TbL4}$  ( $c = 10^{-6}$  M), prepared in the previous experiments, upon exposure to UV light at 254 nm. Radiolabeling with  $^{161}\text{Tb}$  was, therefore, performed with 20 nmol of **L4** and the remaining free ligand was then saturated with natural (non-radioactive) terbium ( $^{\text{nat}}\text{Tb}$ ). This enabled the use of a final concentration of  $10^{-4}$  M  $^{\text{nat}/161}\text{TbL4}$ . The reaction vial containing the  $\text{TbL4}$  complex was exposed to UV light at 254 nm, which resulted in a fluorescent emission of the  $\text{TbL4}$  complex (Figure 7).

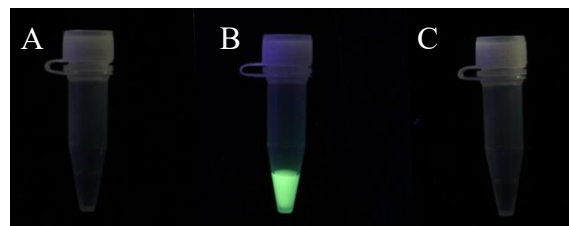


**Figure 7.** Radiometal complex vials exposed to 254 nm light: (A)  $^{161}\text{TbL4}$  not saturated ( $c = 10^{-6}$  M), (B)  $^{\text{nat}/161}\text{TbL4}$  saturated with non-radioactive terbium ( $c = 10^{-4}$  M) and (C)  $^{161}\text{TbCl}_3$  solution.

These preliminary experiments suggest the potential of dipicolinate-pyclen ligands that can be used as a bifunctional chelator, in conjunction with a tumor targeting agent, in view of a theranostic application. These ligands can be labeled with  $^{161}\text{Tb}$  for potential application in radionuclide therapy while, on the other hand, natural terbium can be used for optical imaging. The latter may have particular value for intraoperative imaging, enabling the detection of small lesions during surgery.<sup>31</sup> In this field, it was demonstrated that picolinate moieties can be  $\pi$ -extended to allow biphotonic absorption, i.e. in the biological window, for better *in vivo* penetration.<sup>32</sup>

## Conclusion

In the present study, we expanded the scope of picolinate-pyclen-based ligands for the complexation of trivalent lanthanide ions for radionuclide therapy. It was proven that this family of ligands, previously explored in depth, forms thermodynamically and kinetically stable complexes with Tb<sup>3+</sup> and Lu<sup>3+</sup>, even exceeding the properties of the well-known Ln(DOTA) and Ln(PCTA) complexes. The radiolabeling experiments with both <sup>161</sup>Tb and <sup>177</sup>Lu demonstrated the fast and efficient radiometal complexation. Compared to the DOTA radiometal complexes, the pyclen bearing picolinate chelates lead to radiocomplexes with comparable inertness. **L4** is now proposed as a potential candidate to be used with Y<sup>3+</sup> and Ln<sup>3+</sup> radioisotopes for nuclear medicine applications. The optical properties may be a useful additional capacity that DOTA does not present. Coupling to the recent progress in the field of biphotonic absorption,<sup>32</sup> modification of the picolinate unit may allow us to access theranostic systems usable *in vivo* in future

## Experimental Section

### Materials and methods

Reagents used for the synthesis were purchased from Acros Organics or Sigma-Aldrich and used without further purification. Ultrapure water was freshly obtained from a Milli-Q dispenser. A solvent purification system was used to dispense dry solvents before each reaction. NMR spectra were recorded at the “Services communs” of the University of Brest. <sup>1</sup>H and <sup>13</sup>C NMR spectra were recorded using Bruker Avance 500 (500 MHz), Bruker Avance 400 (400 MHz) or Bruker AMX-300 (300 MHz) spectrometers. Coupling constants are given in Hertz and chemical shifts in ppm. HRMS analysis were carried out on a HRMS Q-ToF MaXis instrument equipped with ESI, APCI, APPI, and nano-ESI sources at the Institute of Organic and Analytic Chemistry – ICOA in Orléans, France.

### Synthesis of ML complexes

General procedure for preparation of ML chelates is as follows:

**L2**·HCl was dissolved in H<sub>2</sub>O (260 μL) and the pH adjusted to ~6 with 1.0 M KOH solution (~50 μL). A solution of MCl<sub>3</sub>·6H<sub>2</sub>O in H<sub>2</sub>O (C=0.5 M) was added to the ligand solution and KOH (1.0 M; ~50 μL) were added again to obtain a pH of ~5. The mixture was heated at 90 °C for 4 hours and then concentrated. The complex was taken up in methanol (500 μL) and filtered twice to remove salts. After evaporation, the desired complex was obtained in quantitative yield.

Detailed quantities and characterization are provided in Supporting Information.

### Single crystal X-ray diffraction measurements.

Crystallographic data were collected at 193(2) K on a Bruker-AXS Kappa APEX II Quazar diffractometer equipped with a 30W air-cooled microfocus source (**LuL3** and **TbL3**), using MoK<sub>α</sub> radiation (λ=0.71073 Å) or on a Bruker-AXS D8-Venture equipped with a CMOS Area detector and a 30W air-cooled microfocus source (**LuL4** and **TbL4**), using CuK<sub>α</sub> radiation (λ=1.54178 Å). Phi- and omega-scans were used.

Space groups were determined on the basis of systematic absences and intensity statistics. Semi-empirical absorption correction was employed.<sup>33</sup> The structures were solved using an intrinsic phasing method (SHELXT),<sup>34</sup> and refined using the least-squares method on  $F^2$ .<sup>35</sup> All non-H atoms were refined with anisotropic displacement parameters. Hydrogen atoms were refined isotropically at calculated positions using a riding model with their isotropic displacement parameters constrained to be equal to 1.5 times the equivalent isotropic displacement parameters of their pivot atoms for terminal *sp*<sup>3</sup> carbon and 1.2 times for all other carbon atoms. All H atoms of H<sub>2</sub>O molecules were located by difference Fourier map and some restraints were applied on bond lengths and angles: SADI, DFIX, DANG. Some residual electron density were difficult to modelize (**LuL4**) and therefore, the SQUEEZE function of PLATON<sup>36</sup> was used to eliminate the contribution of the electron density in the solvent region from the intensity data, and the solvent-free model was employed for the final refinement. CCDC-1992259 (**LuL3**), CCDC-1992260 (**LuL4**), CCDC-1992261 (**TbL3**) and CCDC-1992262 (**TbL4**) contain the supplementary crystallographic data for this paper. These data can be obtained free of charge from The Cambridge Crystallographic Data Centre via [www.ccdc.cam.ac.uk/data\\_request/cif](http://www.ccdc.cam.ac.uk/data_request/cif).

**DFT calculations.** Density functional theory (DFT) calculations on the **LuL3** and **LuL4** complexes were carried out with the g09 program package within the hybrid-meta GGA approximation with the TPSSh functional.<sup>37,38</sup> Geometry optimizations were followed by analytical frequency calculations to establish the nature of the optimized structures as true energy minima. Bulk solvent effects (water) were considered with the integral equation formalism variant of the polarized continuum model (IEFPCM) using the default radii internally stored in g09 to describe the solute cavities.<sup>39</sup> Relativistic effects were considered with the aid of the small-core quasi-relativistic effective core potential of Dolg *et al.*, which includes 28 electrons in the core for the lanthanides, and the related ECP28MWB\_GUESS basis set.<sup>40</sup> The ligand atoms were described using the standard 6-31(d,p) basis set.

### Potentiometry

**Equipment and working conditions.** The potentiometric setup consisted of a 50 mL glass-jacketed titration cell sealed from the atmosphere and connected to a separate glass-jacketed reference electrode cell by a Wilhelm type salt bridge filled with 0.1 M KNO<sub>3</sub> electrolyte. A Metrohm 6.0262.100 combined glass electrode was used for the measurements. The ionic strength of the experimental solutions was kept at 0.10 ± 0.01 M with KNO<sub>3</sub>; temperature was controlled at 298.2 ± 0.1 K using a Lauda E100 cooling and heating bath thermostat. Atmospheric CO<sub>2</sub> was excluded from the titration cell during experiments by slightly bubbling purified nitrogen through the experimental solution. Titrant solutions were added through capillary tips at the surface of the experimental solution by a Metrohm Dosimat 888 automatic burette. Titration procedure is automatically controlled by software after the selection of suitable parameters, allowing for long unattended experimental runs. The titrant was a ~0.1 M KOH solution prepared

from a commercial ampoule of analytical grade KOH, and its accurate concentration was obtained by application of the Gran's method<sup>41</sup> upon titration of a standard HNO<sub>3</sub> solution. Ligand solution was prepared at *ca.*  $2.0 \times 10^{-3}$  M, and the Tb<sup>3+</sup> and Lu<sup>3+</sup> solutions were prepared at *ca.* 0.04 M (containing 0.05 M HNO<sub>3</sub>) from analytical grade hydrated chlorides and standardized by complexometric titrations with H<sub>4</sub>EDTA (ethylenediaminetetraacetic acid). Sample solutions for titration contained approximately 0.05 mmol of ligand in a volume of 30 mL. In complexation titrations, metal cations were added at 0.1 equivalent of the ligand amount. Batch competition titration in the intermediate pH range (3 to 11) contained approximately 0.005 mmol of ligand in a volume of 3 mL with DOTA and metal cation added both at 1 equivalent of ligand amount. Increasing amounts of standardized KOH solution at *ca.* 0.1 M were added to each one. Batch titration points were incubated in tightly closed vials at 25 °C in a Lauda Alpha RA 24 thermostat until potential measurements attained complete stability (about four weeks).

**Measurements.** The electromotive force of the sample solutions was measured after calibration of the electrode by titration of a standard HNO<sub>3</sub> solution at  $2.0 \times 10^{-3}$  M. The [H<sup>+</sup>] of the solutions was determined by measurement of the electromotive force of the cell,  $E = E^{\circ'} + Q \log [H^+] + E_j$ . The term pH is defined as  $-\log[H^+]$ .  $E^{\circ'}$  and  $Q$  were determined from acid region of the calibration curves. The liquid-junction potential,  $E_j$ , was found to be negligible under the experimental conditions used. The value of  $K_w = [H^+][OH^-]$  was found to be equal to  $10^{-13.78}$  by titrating a solution of known hydrogen-ion concentration at the same ionic strength in the alkaline pH region, considering  $E^{\circ'}$  and  $Q$  valid for the entire pH range. The protonation constants of DOTA and the thermodynamic stability constants of its Tb<sup>3+</sup> and Lu<sup>3+</sup> complexes used in competition titration refinements were taken from the literature.<sup>9(b)</sup>

**Calculations.** The potentiometric data were refined with the HYPERQUAD software,<sup>42</sup> and speciation diagrams were plotted using the HySS software.<sup>43</sup> The overall equilibrium constants  $\beta_i^H$  and  $\beta_{MmHhLi}$  are defined by  $\beta_{MmHhLi} = [M_mH_hL_i]/[M]^m[H]^h[L]^l$  ( $\beta_i^H = [H_iL_i]/[H]^h[L]^l$  and  $\beta_{MH-IL} = \beta_{ML(OH)} \times K_w$ ). Differences, in log units, between the values of protonated (or hydrolyzed) and non-protonated constants provide the stepwise (log  $K$ ) reaction constants (being  $K_{MmHhLi} = [M_mH_hL_i]/[M_mH_{h-1}L_i][H]$ ). The errors quoted are the standard deviations calculated by the fitting program from all the experimental data for each system. Batch competition titration allow us to determine the  $K_{ML}$  constant.  $K_{MLH}$  and  $K_{MLH-1}$  constants were determined with the refinement of direct titration measurements.

### Radiolabeling and stability studies.

Terbium-161 chloride (<sup>161</sup>TbCl<sub>3</sub>) was purified at PSI after target irradiation at NeCSA (South African Nuclear Energy Corporation SOC Limited), South Africa, or ILL (Institut Laue-Langevin), France, as previously reported,<sup>44</sup> while lutetium-177 chloride (<sup>177</sup>LuCl<sub>3</sub>) was provided by ITG (Isotopes Technologies Garching GmbH, Germany). All chemicals used

for the radiolabeling were virtually metal-free (trace analysis grade) and obtained from Merck (Germany) in Suprapur quality. Other reagents and solvents were purchased from Sigma-Aldrich (Germany), Merck (Germany), and Fluka (Switzerland), and used without further purification or drying.

### Preparation of radiometal complexes

Each ligand, **L2**, **L3**, **L4** and DOTA, was labeled at molar activities of 5 MBq/nmol and 50 MBq/nmol with either <sup>161</sup>Tb or <sup>177</sup>Lu. These molar activities corresponded to a chelator-to-radionuclide ratio of about 140:1 for 5 MBq/nmol and 14:1 for 50 MBq/nmol, respectively. The radionuclides were added to a reaction mixture consisting of 0.05 M HCl and 0.5 M sodium acetate in a 5:1 (*v/v*) ratio to obtain a solution of pH  $\approx$  4.5. After the addition of the ligand in question (stock solutions of 1 mM in Milli-Q water), the reaction mixture was incubated at 95 °C for 10 min.<sup>45</sup> The quality control of the radiometal complexes was carried out *via* thin layer chromatography (TLC), applying a previously-reported method [using silica gel 60 F<sub>254</sub> plates ( $\sim 100 \times 100$  mm<sup>2</sup>).<sup>46</sup> As a mobile phase, 10% ammonium acetate and methanol (1:1 (*v/v*), pH 5.5) was used. Elution proceeded over 55 mm from the baseline to the front line. For this purpose, radiometal complexes diluted at 0.15 MBq/ $\mu$ L were pipetted (2  $\mu$ L) onto the TLC plate. The <sup>161</sup>Tb- and <sup>177</sup>Lu-labeled DOTA complex migrated with the liquid phase ( $R_f = 0.4$ ) and non-chelated <sup>161</sup>Tb and <sup>177</sup>Lu remained at the start line ( $R_f = 0$ ). Retention of the <sup>161</sup>Tb-labeled **L2**, **L3** and **L4** or <sup>177</sup>Lu-labeled **L2**, **L3** and **L4** was determined at  $R_f = 0.2$ . The TLC plate was exposed to a super resolution phosphor screen (Type MS, PerkinElmer, Waltham MA, U.S.A.) for 15 seconds, which was then read using a Cyclone Plus Storage Phosphor System (PerkinElmer, Waltham MA, U.S.A.) and analyzed with Optiquant software (version 5.0). Quantifications of the TLC signals with the indicated software enabled the determination of intact radiometal complex over total activity in the different conditions of the experiments.

### Stability of radiometal complexes

The stability of the radiometal complexes was investigated under various conditions. The <sup>161</sup>Tb-labeled complexes were studied after radiolabeling at 50 MBq/nmol and dilution in Milli-Q water, saline or PBS. The activity concentration was 0.15 MBq/ $\mu$ L in a total volume of 160  $\mu$ L and the solutions were incubated for 4 hours, 1 day, 2 days, 3 days and 4 days, respectively, at room temperature. At each time point the fraction of intact radiometal complex was quantified using TLC, according to the method described above, and expressed as percentage of intact product after setting the total activity to 100%.

The same procedure was performed with <sup>161</sup>Tb**L2**, after labeling at 5 MBq/nmol molar activity to assess whether the radiometal complex would be less prone to radiolysis at lower molar activity.

The stability of the radiometal complexes was also investigated at the same activity concentration in the presence of ethanol or ascorbic acid as scavengers. After radiolabeling at 50 MBq/nmol molar activity with either <sup>161</sup>Tb or <sup>177</sup>Lu, the radiometal complexes were diluted (0.15 MBq/ $\mu$ L in a final vol-

ume of 160  $\mu\text{L}$ ) in saline or PBS, with the addition of 15  $\mu\text{L}$  absolute ethanol (<10% of the total final volume) or 15  $\mu\text{L}$  ascorbic acid (0.11 M in Milli-Q water) and incubated at room temperature. The intact radiometal complex was investigated at 4 hours, 1 day, 2 days, 3 days and 7 days after radiolabeling, respectively, using TLC.

#### *Kinetic inertness investigated with challenging agents*

The stability of the  $^{161}\text{Tb}$ - and  $^{177}\text{Lu}$ -radiometal complexes was investigated in the presence of an excess of coordinating species (DTPA and EDTA), so that the competitor was in 1000-fold molar excess compared to the radiometal complex. An aliquot of each radiometal complex (50 MBq/nmol; 30  $\mu\text{L}$ ) was diluted in saline in the presence of DTPA or EDTA (40  $\mu\text{L}$ , 50 mM, pH 5.0) and absolute ethanol (15  $\mu\text{L}$ ) at an activity concentration of 0.15 MBq/ $\mu\text{L}$  and a final volume of 160  $\mu\text{L}$ . The intact radiometal complexes were determined, with the TLC method described above, as a function of time ( $t=0$ , 4 hours, 1 day, 2 days, 3 days and 7 days) after incubating the  $^{161}\text{Tb}$  and  $^{177}\text{Lu}$  radiometal complexes at room temperature in the presence of the challenging ligands.

The stability of the radiometal complexes was also investigated in the presence of a large excess of metallic species ( $\text{Fe}^{2+}$  and  $\text{Zn}^{2+}$ ), maintaining the metal ion-to-radiometal complex molar ratio equal to 1000. The intact radiometal complexes were determined, with the TLC method described above, as a function of time ( $t=0$  h, 4 h, 1 day, 2 days, 3 days and 7 days) after incubating the  $^{161}\text{Tb}$  and  $^{177}\text{Lu}$  radiometal complexes at room temperature in the presence of the challenging metal ions.

#### *Determination of radiolabeling kinetics at 37° C*

Labeling kinetics were studied for  $^{161}\text{TbL4}$ ,  $^{177}\text{LuL4}$  and their DOTA analogue, using the methods described above, to achieve radiolabeling at 50 MBq/nmol. The radiolabeling was carried out in a total volume of 120  $\mu\text{L}$  and in the presence of ~10% absolute ethanol (12  $\mu\text{L}$ ). The radiolabeling mixture was incubated for 10 minutes, 30 minutes, or 1 hour at 37 °C. At each time point, 10  $\mu\text{L}$  of the labeling solution was pipetted and measured (Isomed Dose Calibrator 2010 device). The aliquots were diluted with saline solution (~40  $\mu\text{L}$ ) in order to obtain an activity of 0.15 MBq/ $\mu\text{L}$ . The radiolabeled product relative to the total activity determined on the TLC plate was indicated as radiolabeling yield (RCY) at each investigated time point.

#### *Evaluation of TbL4 emission*

An initial experiment to show the  $^{161}\text{Tb}^{3+}$ -complex emission under UV light at 254 nm was performed. As a proof of concept, the most promising radiometal complex,  $^{161}\text{TbL4}$ , was tested by exposing it to UV light. To see the luminescence of the  $\text{Tb}^{3+}$  complex in solution, it is necessary to use a concentration higher than  $10^{-5}$  M of complexed lanthanide.  $^{161}\text{TbL4}$ , prepared as described above, was at a concentration of around  $10^{-6}$  M of chelated radiometal and, therefore, does not show visible fluorescence. In an additional experiment, **L4** (20 nmol) was labeled with 100 MBq  $^{161}\text{Tb}$  following the standard labeling method described above. Afterwards,  $^{161}\text{TbL4}$  was incubated with 60  $\mu\text{L}$  of a

1mM natural (non-active) terbium solution ( $^{\text{nat}}\text{TbCl}_3$ ) and the reaction mixture heated again at 95 °C for 10 minutes. This procedure enabled the occupation of each **L4** ligand molecule by a terbium metal ion and achieve a final concentration of  $10^{-4}$  M  $^{\text{nat}/161}\text{TbL4}$ . To assess the photoluminescence emission, the  $^{\text{nat}/161}\text{TbL4}$  complex was exposed to UV light at 254 nm and potential luminescence was compared with the  $^{161}\text{TbL4}$  complex labeled at 50 MBq/nmol and the  $^{161}\text{TbCl}_3$  solution.

## ASSOCIATED CONTENT

**Supporting Information.** Syntheses, HR-MS spectra, NMR spectra, X-ray data, UV-vis spectra from dissociation experiments, DFT calculations, speciation diagrams,  $^{161}\text{Tb}$ - and  $^{177}\text{Lu}$ -complexes stabilities,  $^{177}\text{Lu}$ -complexes transmetallation and transchelation. This material is available free of charge via the Internet at <http://pubs.acs.org>.

## AUTHOR INFORMATION

### Corresponding Author

\* Prof. Dr. Raphael Tripier; [raphael.tripier@univ-brest.fr](mailto:raphael.tripier@univ-brest.fr)  
\* Dr. Maryline Beyler; [Maryline.Beyler@univ-brest.fr](mailto:Maryline.Beyler@univ-brest.fr)

### ORCID

Gwladys Nizou: 0000-0001-9829-9327  
Chiara Favaretto: 0000-0003-2096-8994  
Francesca Borgna: 0000-0002-5471-0767  
Pascal V. Grundler : 0000-0002-1872-7764  
Nathalie Saffon-Merceron: 0000-0002-0301-4163  
Carlos Platas-Iglesias: 0000-0002-6989-9654  
Nicholas P. van der Meulen: 0000-0001-6077-5594  
Cristina Müller : 0000-0001-9900-1959  
Maryline Beyler: 0000-0002-6540-970X  
Raphaël Tripier: 0000-0001-9364-788X

### Author Contributions

The manuscript was written through contributions of all authors. / All authors have given approval to the final version of the manuscript.

## ACKNOWLEDGEMENTS

R.T. and M. B. acknowledge the Ministère de l'Enseignement Supérieur et de la Recherche and the Centre National de la Recherche Scientifique. They also thank the "Service Commun" of NMR facilities of the University of Brest. R. T., M. B. and O. R. also thank the Guerbet group and the Association Nationale de la Recherche et de la Technologie for the CIFRE fellowship of G. N. C. P.-I. thanks Centro de Supercomputación de Galicia for providing access to computing facilities.

G. N. acknowledges the Paul Scherrer Institute and the Guerbet group for the 2 months of short mission in Villigen in 2019.

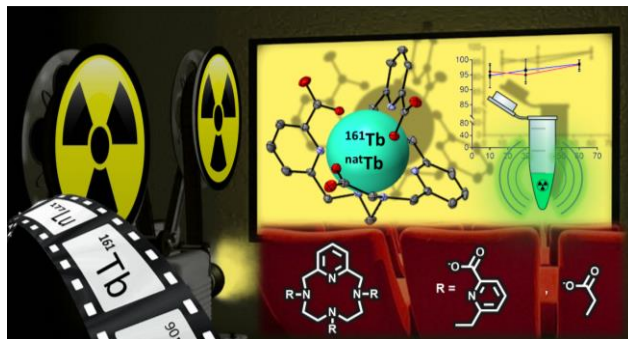
C.M. and N.vdM. acknowledge Fan Sozzi-Guo for assistance of the experiments involving  $^{161}\text{Tb}$ .

## REFERENCES

- (1) Caravan, P.; Ellison, J. J.; McMurry, T. J.; Lauffer, R. B. Gadolinium(III) Chelates as MRI Contrast Agents: Structure, Dynamics, and Applications. *Chem. Rev.* **1999**, *99*, 2293–2352.
- (2) Eliseeva, S. V.; Bünzli, J.-C. G. Lanthanide luminescence for functional materials and bio-sciences. *Chem. Soc. Rev.* **2010**, *39*, 189–227
- (3) Müller, C.; Zhernosekov, K.; Köster, U.; Johnston, K.; Dorrer, H.; Hohn, A.; van der Walt, N. T.; Türlér, A.; Schibli, R. A Unique Matched Quadruplet of Terbium Radioisotopes for PET and SPECT and for  $\alpha$ - and  $\beta$ -Radionuclide Therapy: An In Vivo Proof-of-Concept Study with a New Receptor-Targeted Folate Derivative. *J. Nucl. Med.* **2012**, *53*, 1951-1959;
- (4) (a) Banerjee, S.; Pillai, M. R. A.; Knapp, F. F. Lutetium-177 Therapeutic Radiopharmaceuticals: Linking Chemistry, Radiochemistry, and Practical Applications. *Chem. Rev.* **2015**, *115*, 2934-2974; (b) Das, T.; Banerjee, S. Theranostic Applications of Lutetium-177 in Radionuclide Therapy. *Curr Radiopharm.* **2016**, *9*, 94-101; (c) Müller C.; Umbricht CA.; Gracheva, N.; Tschan, V. J.; Pellegrini, G.; Bernhardt, P.; Zeevaert, J. R.; Köster, U.; Schibli, R.; van der Meulen, N. P. Terbium-161 for PSMA-targeted radionuclide therapy of prostate cancer. *Eur. J. Nucl. Med. Mol. Imaging* **2019**, *46*, 1919-1930; (e) Klaassen, N. J. M.; Arntz, M. J.; Gil Arranja, A.; Roosen, J.; Nijsen, J. F. W. The various therapeutic applications of the medical isotope holmium-166: a narrative review. *EJNMMI radiopharm. chem.* **2019**, 4:19.
- (5) Kennedy, A. S.; Nutting, C.; Coldwell, D.; Gaiser, J.; Drachenberg, C. Pathologic response and microdosimetry of  $^{90}\text{Y}$  microspheres in man: Review of four explanted whole livers. *Int. J. Rad. Oncol. Biol. Phys.* **2004**, *60*, 1552-1563.
- (6) Johnson, L. S.; Yanch, J. C. Absorbed dose profiles for radionuclides of frequent use in radiation synovectomy. *Arthritis and Rheumatism* **1991**, *34*, 1521-1530.
- (7) Hennrich, U.; Kopka, K. Lutathera®: The First FDA- and EMA-Approved Radiopharmaceutical for Peptide Receptor Radionuclide Therapy. *Pharmaceuticals* **2019**, *12*, 114-122.
- (8) Durán, M. T.; Juget, F.; Nedjadi, Y.; Bochud, F.; Grundler, P. V.; Gracheva, N.; Müller, C.; Talip, Z.; van der Meulen, N. P.; Bailat, C. Determination of  $^{161}\text{Tb}$  half-life by three measurement methods. *Appl. Rad. and Isot.* **2020**, *159*, article 109085.
- (9) (a) Loncin, M. F.; Desreux, J. F.; Merciny, E. Metal-nitroxyl interactions. 47. EPR spectra of two-spin-labeled derivatives of EDTA coordinated to paramagnetic metal ions. *Inorg. Chem.* **1986**, *25*, 2646-2648; (b) Cacheris, W. P.; Nickle, S. K.; Sherry, A. D. Thermodynamic study of lanthanide complexes of 1,4,7-triazacyclononane-N,N',N''-triacetic acid and 1,4,7,10-tetraazacyclododecane-N,N',N'',N'''-tetraacetic acid. *Inorg. Chem.* **1987**, *26*, 958-960; (c) Tóth, E.; Brücher, E.; Lázár, I.; Tóth, I. Kinetics of Formation and Dissociation of Lanthanide(III)-DOTA Complexes. *Inorg. Chem.* **1994**, *33*, 4070-4076.
- (10) Beeby, A.; Clarkson, I. M.; Dickens, R. S.; Faulkner, S.; Parker, D.; Royle, L.; de Sousa, A. S.; Williams, J. A. G.; Woods, M. Non-radiative deactivation of the excited states of europium, terbium and ytterbium complexes by proximate energy-matched OH, NH and CH oscillators: an improved luminescence method for establishing solution hydration states. *J. Chem. Soc., Perkin Trans. 2* **1999**, 493-504.
- (11)(a) Sherry, A. D. MR imaging and spectroscopy applications of lanthanide complexes with macrocyclic phosphonate and phosphonate ester ligands. *J. Alloys Compd.* **1997**, *249*, 153-157; (b) Parker, D. Luminescent lanthanide sensors for pH, pO<sub>2</sub> and selected anions. *Coord. Chem. Rev.* **2000**, *205*, 109-130; (c) Chalmers, K. H.; De Luca, E.; Hogg, N. H. M.; Kenwright, A. M.; Kuprov, I.; Parker, D.; Botta, M.; Wilson, J. I.; Blamire, A. M. Design Principles and Theory of Paramagnetic Fluorine-Labelled Lanthanide Complexes as Probes for  $^{19}\text{F}$  Magnetic Resonance: A Proof-of-Concept Study. *Chem. - Eur. J.* **2010**, *16*, 134-148; (d) Ur Rashid, H.; Utrera Martines, M. A.; Jorge, J.; Martin de Moraes, P.; Umar, M. N.; Khan, K.; Ur Rehman, H. Cyclen-based Gd<sup>3+</sup> complexes as MRI contrast agents: Relaxivity enhancement and ligand design. *Bioorg. Med. Chem.* **2016**, *24*, 5663–5684; (e) Bui, A. T.; Beyler, M.; Liao, Y.-Y.; Grichine, A.; Duperray, A.; Mulatier, J.-C.; Le Guennic, B.; Andraud, C.; Maury, O.; Tripiet, R. Cationic Two-Photon Lanthanide Bioprobes Able to Accumulate in Live Cells. *Inorg. Chem.* **2016**, *55*, 7020-7025.
- (12)(a) Werner, E. J.; Avedano, S.; Botta, M.; Hay, B. P.; Moore, E. G.; Aime, S.; Raymond, K. N. Highly Soluble Tris-hydroxypyridonate Gd(III) Complexes with Increased Hydration Number, Fast Water Exchange, Slow Electronic Relaxation, and High Relaxivity. *J. Am. Chem. Soc.* **2007**, *129*, 1870-1871; (b) Nocton, G.; Nonat, A.; Gateau, C.; Mazzanti, M. Water Stability and Luminescence of Lanthanide Complexes of Tripodal Ligands Derived from 1,4,7-Triazacyclononane: Pyridinecarboxamide versus Pyridinecarboxylate Donors. *Helv. Chim. Acta* **2009**, *92*, 2257-2273; (c) Walton, J. W.; Bourdolle, A.; Butler, S. J.; Soulie, M.; Delbianco, M.; McMahon, B. K.; Pal, R.; Puschmann, H.; Zwier, J. M.; Lamarque, L.; Maury, O.; Andraud, C.; Parker, D. Very bright europium complexes that stain cellular mitochondria. *Chem. Commun.* **2013**, *49*, 1600-1602; (d) Butler, S. J.; Lamarque, L.; Pal, R.; Parker, D. EuroTracker dyes: highly emissive europium complexes as alternative organelle stains for live cell imaging. *Chem. Sci.* **2014**, *5*, 1750-1756; (e) D'Aléo, A.; Bourdolle, A.; Brustlein, S.; Fauquier, T.; Grichine, A.; Duperray, A.; Baldeck, P. L.; Andraud, C.; Brasselet, S.; Maury, O. Ytterbium-based bioprobes for near-infrared two-photon scanning laser microscopy imaging. *Angew. Chem., Int. Ed.* **2012**, *51*, 6622-6625.
- (13) (a) Saudan, C.; Ceroni, P.; Vicinelli, V.; Maestri, M.; Balzani, V.; Gorka, M.; Lee, S.-K.; van Heyst, J.; Vögtle, F. Cyclam-based dendrimers as ligands for lanthanide ions. *Dalton Trans.* **2004**, 1597-1600; (b) Pillai, Z. S.; Ceroni, P.; Kubeil, M.; Heldt, J.-M.; Stephan, H.; Bergamini, G. Dendrimers as Nd<sup>3+</sup> ligands: Effect of Generation on the Efficiency of the Sensitized Lanthanide Emission. *Chem. Asian J.* **2013**, *8*, 771-777; (c) Rodríguez-Rodríguez, A.; Esteban-Gómez, D.; Tripiet, R.; Tircsó, G.; Garda, Z.; Tóth, I.; de Blas, A.; Rodríguez-Blas, T.; Platas-Iglesias, C. Lanthanide(III) Complexes with a Reinforced Cyclam Ligand Show Unprecedented Kinetic Inertness. *J. Am. Chem. Soc.* **2014**, *136*, 17954-17957; (d) Mendy, J.; Bui, A. T.; Roux, A.; Mulatier, J.-C.; Curton, D.; Duperray, A.; Grichine, A.; Guyot, Y.; Brasselet, S.; Riobé, F.; Andraud, C.; Le Guennic, B.; Patinec, V.; Tripiet, R.; Beyler, M.; Maury, O. Cationic Biphononic Lanthanide Luminescent Bioprobes Based on Functionalized Cross-Bridged Cyclam Macrocycles. *ChemPhysChem* **2020**, doi-org.inc.bib.cnrs.fr/10.1002/cphc.202000085
- (14) Tircsó, G.; Kovács, Z.; Sherry, A. D. Equilibrium and formation/dissociation kinetics of some Ln<sup>III</sup>PCTA complexes. *Inorg. Chem.* **2006**, *45*, 9269-9280.
- (15)(a) Aime, S.; Botta, M.; Crich, S. G.; Giovenzana, G. B.; Jommi, G.; Pagliarini, R.; Sisti, M. Synthesis and NMR Studies of Three Pyridine-Containing Triaza Macrocyclic Triacetate Ligands and Their Complexes with Lanthanide Ions. *Inorg. Chem.* **1997**, *36*, 2992–3000; (b) Aime, S.; Botta, M.; Crich, S. G.; Giovenzana, G.; Pagliarini, R.; Sisti, M.; Terreno, E. NMR relaxometric studies of Gd(III) complexes with heptadentate macrocyclic ligands. *Magn. Reson. Chem.* **1998**, *36*, S200–S208. (c) Port, M.; Raynal, I.; Vander Elst, L.; Muller, R. N.; Dioury, F.; Ferroud, C.; Guy, A. Impact of rigidification on relaxometric properties of a tricyclic tetraazatriacetic gadolinium chelate. *Contrast Media Mol. Imaging* **2006**, *1*, 121–127. (d) Rojas-Quijano, F. A.; Benyó, E. T.; Tircsó, G.; Kálmán, F. K.; Baranyai, Z.; Aime, S.; Sherry, D. A.; Kovács, Z. Lanthanide(III) Complexes of Tris(amide) PCTA Derivatives as Potential Bimodal Magnetic Resonance and Optical Imaging Agents. *Chem. - Eur. J.* **2009**, *15*, 13188–13200. (e) Bort, G.; Catoen, S.; Borderies, H.; Kebbi, A.; Ballet, S.; Louin, G.; Port, M.; Ferroud, C. Gadolinium-based contrast agents

- targeted to amyloid aggregates for the early diagnosis of Alzheimer's disease by MRI. *Eur. J. Med. Chem.* **2014**, *87*, 843–861.
- (16)(a) Le Fur, M.; Beyler, M.; Molnár, E.; Fougère, O.; Esteban-Gómez, D.; Tircsó, G.; Platas-Iglesias, C.; Lepareur, N.; Rousseaux, O.; Tripier, R. The role of the capping bond effect on pyclen  $^{nat}Y^{3+}/^{90}Y^{3+}$  chelates: Full control of the regioselective N-functionalization makes the difference. *Chem. Commun.* **2017**, *53*, 9534–9537; (b) Le Fur, M.; Beyler, M.; Molnár, E.; Fougère, O.; Esteban-Gómez, D.; Tircsó, G.; Platas-Iglesias, C.; Lepareur, N.; Rousseaux, O.; Tripier, R. Stable and Inert Yttrium(III) Complexes with Pyclen-Based Ligands Bearing Pendant Picolinate Arms: Toward New Pharmaceuticals for  $\beta$ -Radiotherapy. *Inorg. Chem.* **2018**, *57*, 2051–2063; (c) Le Fur, M.; Molnár, E.; Beyler, M.; Kálmán, F. K.; Fougère, O.; Esteban-Gómez, D.; Rousseaux, O.; Tripier, R.; Tircsó, G.; Platas-Iglesias, C. A Coordination Chemistry Approach to Fine-Tune the Physicochemical Parameters of Lanthanide Complexes Relevant to Medical Applications. *Chem.-Eur. J.* **2018**, *24*, 3127–3131; (d) Le Fur, M.; Molnár, E.; Beyler, M.; Fougère, O.; Esteban-Gómez, D.; Rousseaux, O.; Tripier, R.; Tircsó, G.; Platas-Iglesias, C. Expanding the Family of Pyclen-Based Ligands Bearing Pendant Picolinate Arms for Lanthanide Complexation. *Inorg. Chem.* **2018**, *57*, 6932–6945, (e) Le Fur, M.; Tripier, R.; Rousseaux, O.; Beyler, M. Macrocyclic ligands with picolinate groups, their complexes like their medical uses. Patent n° WO 2017109217, Application n° WO 2016-EP82644.
- (17)Spek, A. L. PLATON SQUEEZE: a tool for the calculation of the disordered solvent contribution to the calculated structure factors. *Acta Crystallogr. Sect. C* **2015**, *71*, 9–18.
- (18)Ruiz-Martínez, A.; Casanova, D.; Alvarez, S. Polyhedral Structures with an Odd Number of Vertices: Nine-Coordinate Metal Compounds. *Chem.-Eur. J.*, **2008**, *14*, 1291–1303
- (19)Dale, J. Exploratory Calculations of Medium and Large Rings. Part 2. Conformational Interconversions in Cycloalkanes. *Acta Chem. Scand.* **1973**, *27*, 1130–1148.
- (20)Kiefer, G. E.; Woods, M. Solid State and Solution Dynamics of Pyridine Based Tetraaza-Macrocyclic Lanthanide Chelates Possessing Phosphonate Ligating Functionality (Ln-PCTMB): Effect on Relaxometry and Optical Properties. *Inorg. Chem.* **2009**, *48*, 11767–11778.
- (21)Beattie, J. K. Conformational analysis of tris(ethylenediamine) complexes. *Acc. Chem. Res.* **1971**, *4*, 253–259.
- (22)Shannon, R. D. Revised effective ionic radii and systematic studies of interatomic distances in halides and chalcogenides; *Acta Crystallogr. Sect. A* **1976**, *32*, 751–767.
- (23)Seitz, M.; Oliver, A. G.; Raymond, K. N. The Lanthanide Contraction Revisited. *J. Am. Chem. Soc.* **2007**, *129*, 11153–11160.
- (24) (a) Price, E. W.; Zeglis, B. M.; Cawthray, J. F.; Lewis, J. S.; Adam, M. J.; Orvig, C. H<sub>4</sub>octapa-Trastuzumab: Versatile Acyclic Chelate System for <sup>111</sup>In and <sup>177</sup>Lu Imaging and Therapy. *J. Am. Chem. Soc.* **2013**, *135*, 12707–12721; (b) Price, E. W.; Zeglis, B. M.; Cawthray, J. F.; Ramogida, C. F.; Ramos, N.; Lewis, J. S.; Adam, M. J.; Orvig, C. What a Difference a Carbon Makes: H<sub>4</sub>octapa vs H<sub>4</sub>C<sub>3</sub>octapa, Ligands for In-111 and Lu-177 Radiochemistry. *Inorg. Chem.* **2014**, *53*, 10412–10431.
- (25)Rojas-Quijano, F.; Benyó, E. T.; Tircsó, G.; Kálmán, F.; Baranyai, Z.; Aime, S.; Sherry, A. D.; Kovács, Z. Lanthanide(III) Complexes of Tris(amide) PCTA Derivatives as Potential Bimodal Magnetic Resonance and Optical Imaging Agents. *Chem. - Eur. J.* **2009**, *15*, 13188–13200.
- (26)Delgado, R.; Frausto Da Silva, J. J. R. Metal complexes of cyclic tetra-azatetra-acetic acids. *Talanta* **1982**, *29*, 815–822.
- (27)Broan, C. J.; Cox, J. P. L.; Craig, A. S.; Katakya, R.; Parker, D.; Harrison, A.; Randall, A. M.; Ferguson, G. Structure and solution stability of indium and gallium complexes of 1,4,7-triazacyclononanetriacetate and of yttrium complexes of 1,4,7,10-tetraazacyclododecanetetraacetate and related ligands: kinetically stable complexes for use in imaging and radioimmunotherapy. X-Ray molecular structure of the indium and gallium complexes of 1,4,7-triazacyclononanetriacetate. *J. Chem. Soc., Perkin Trans. 2* **1991**, 87–99.
- (28) Song, I. H.; Lee, T. S.; Park, Y. S.; Lee, J. S.; Lee, B. C.; Moon, B. S.; An, G. I.; Lee, H. W.; Kim, K. I.; Lee, Y. J.; Kang, J. H.; Lim, S. M. Immuno-PET Imaging and Radioimmunotherapy of <sup>64</sup>Cu-/<sup>177</sup>Lu-Labeled Anti-EGFR Antibody in Esophageal Squamous Cell Carcinoma Model. *J. Nucl. Med.* **2016**, *57*, 1105–1111.
- (29)(a) Regueiro-Figueroa, M.; Esteban-Gómez, D.; de Blas, A.; Rodríguez-Blas, T.; Platas-Iglesias, C. Understanding Stability Trends along the Lanthanide Series. *Chem. Eur. J.* **2014**, *20*, 3974–3981; (b) Thiele, N. A.; Woods, J. J.; Wilson, J. J. Implementing f-Block Metal Ions in Medicine: Tuning the Size Selectivity of Expanded Macrocycles. *Inorg. Chem.* **2019**, *58*, 10483–10500.
- (30) Farkas, E.; Nagel, J.; Waldron, B. P.; Parker, D.; Tjth, I.; Brecher, E.; Rösch, F.; Baranyai, Z. Equilibrium, Kinetic and Structural Properties of Gallium(III) and Some Divalent Metal Complexes Formed with the New DATA<sup>m</sup> and DATA<sup>5m</sup> Ligands. *Chem. Eur. J.* **2017**, *23*, 10358–10371.
- (31) van Dam, G. M.; Themelis, G.; Crane, L. M. A.; Harlaar, N. J.; Pleijhuis, R. G.; Kelder, W.; Sarantopoulos, A.; de Jong, J. S.; Arts, H. J. G., van der Zee, A. G. J.; Bart, J.; Low P. S., Ntziachristos, V. Intraoperative tumor-specific fluorescence imaging in ovarian cancer by folate receptor- $\alpha$  targeting: first in-human results. *Nat. Med.* **2011**, *17*, 1315–1320.
- (32)(a) Hamon, N.; Galland, M.; Le Fur, M.; Roux, A.; Duperray, A.; Grichine, A.; Andraud, C.; Le Guennic, B.; Beyler, M.; Maury, O.; Tripier, R. Combining a pyclen framework with conjugated antenna for the design of europium and samarium luminescent bioprobes. *Chem. Commun.* **2018**, *54*, 6173–6176; (b) Hamon, N.; Roux, A.; Beyler, M.; Mulatier, J.-C.; Andraud, C.; Nguyen, C.; Maynadier, M.; Bettache, N.; Duperray, A.; Grichine, A.; Brasselet, S.; Gary-Bobo, M.; Maury, O.; Tripier R. Pyclen-Based Ln(III) Complexes as Highly Luminescent Bioprobes for In Vitro and In Vivo One- and Two-Photon Bioimaging Applications. *J. Am. Chem. Soc.* **2020** <https://doi.org/10.1021/jacs.0c03496>
- (33)Bruker, SADABS, Bruker AXS Inc., Madison, Wisconsin, USA, **2008**.
- (34)Sheldrick, G. M. SHELXT – Integrated space-group and crystal-structure determination. *Acta Crystallogr. Sect. A* **2015**, *71*, 3–8.
- (35)Sheldrick, G. M. Crystal structure refinement with SHELXL. *Acta Crystallogr. Sect. C* **2015**, *71*, 3–8.
- (36)Spek, A. L. *Acta Crystallogr. Sect. C*, **2015**, *71*, 9–18.
- (37)Frisch, M. J.; Trucks, G. W.; Schlegel, H. B.; Scuseria, G. E.; Robb, M. A.; Cheeseman, J. R.; Scalmani, G.; Barone, V.; Mennucci, B.; Petersson, G. A.; Nakatsuji, H.; Li, X.; Caricato, M.; Marenich, A.; Bloino, J.; Janesko, B. G.; Gomperts, R.; Mennucci, B.; Hratchian, H. P.; Ortiz, J. V.; Izmaylov, A. F.; Sonnenberg, J. L.; Williams-Young, D.; Ding, F.; Lipparini, F.; Egidi, F.; Goings, J.; Peng, B.; Petrone, A.; Henderson, T.; Ranasinghe, D.; Zakrzewski, V. G.; Gao, J.; Rega, N.; Zheng, G.; Liang, W.; Hada, M.; Ehara, M.; Toyota, K.; Fukuda, R.; Hasegawa, J.; Ishida, M.; Nakajima, T.; Honda, Y.; Kitao, O.; Nakai, H.; Vreven, T.; Throssell, K.; Montgomery, Jr., J. A.; Peralta, J. E.; Ogliaro, F.; Bearpark, M.; Heyd, J. J.; Brothers, E.; Kudin, K. N.; Staroverov, V. N.; Keith, T.; Kobayashi, R.; Normand, J.; Raghavachari, K.; Rendell, A.; Burant, J. C.; Iyengar, S. S.; Tomasi, J.; Cossi, M.; Millam, J. M.; Klene, M.; Adamo, C.; Cammi, R.; Ochterski, J. W.; Martin, R. L.; Morokuma, K.; Farkas, O.; Foresman, J. B.; Fox, D. J. Gaussian 09, Revision E.01, Gaussian, Inc.: Wallingford CT, 2009.
- (38) Tao, J. M.; Perdew, J. P.; Staroverov, V. N.; Scuseria, G. E. Climbing the Density Functional Ladder: Nonempirical Meta-Generalized Gradient Approximation Designed for Molecules and Solids. *Phys. Rev. Lett.* **2003**, *91*, 146401.
- (39)Tomasi, J.; Mennucci, B.; Cammi, R. Quantum Mechanical Continuum Solvation Models. *Chem. Rev.* **2005**, *105*, 2999–3093.

- (40) Dolg, M.; Stoll, H.; Preuss, H. Energy-adjusted Ab Initio Pseudopotentials for the Rare Earth Elements. *J. Chem. Phys.* **1989**, *90*, 1730-1734.
- (41) Rossotti, F. J.; Rossotti, H. J. J. Potentiometric titrations using Gran plots: A textbook omission. *Chem. Educ.* **1965**, *42*, 375-378.
- (42) Gans, P.; Sabatini, A.; Vacca, A. Investigation of equilibria in solution. Determination of equilibrium constants with the HYPERQUAD suite of programs. *Talanta* **1996**, *43*, 1739-1753.
- (43) Alderighi, L.; Gans, P.; Ienco, A.; Peters, D.; Sabatini, A.; Vacca, A. Hyperquad simulation and speciation (HySS): a utility program for the investigation of equilibria involving soluble and partially soluble species. *Coord. Chem. Rev.* **1999**, *184*, 311-318.
- (44) Gracheva, N.; Müller, C.; Talip, Z.; Heinitz, S.; Köster, U.; Zeevaert, J.R.; Vögele, A.; Schibli, R.; Van Der Meulen, N. P. Production and characterization of no-carrier-added  $^{161}\text{Tb}$  as an alternative to the clinically-applied  $^{177}\text{Lu}$  for radionuclide therapy. *EJNMMI Radiopharm. Chem.* **2019**, *4*:12, 1-16.
- (45)(a) Müller, C.; Reber, J.; Haller, S.; Dorrer, H.; Bernhardt, P.; Zernosekov, K.; Türlér, A.; Schibli, R. *EJNMMI Radiopharm. Chem.*, 2014, *41*, 476-485; (b) Haller, S.; Pellegrini, G.; Vermeulen, C.; van der Meulen, N. P.; Köster, U.; Bernhardt, P.; Schibli, R.; Müller, C. Contribution of Auger/conversion electrons to renal side effects after radionuclide therapy: preclinical comparison of  $^{161}\text{Tb}$ -folate and  $^{177}\text{Lu}$ -folate. *EJNMMI Res.* **2016**, *6*:13.
- (46) Müller, C.; Farkas, R.; Borgna, F., Schmid, R. M.; Benešová, M.; Schibli, R. Synthesis, Radiolabeling, and Characterization of Plasma Protein-Binding Ligands: Potential Tools for Modulation of the Pharmacokinetic Properties of (Radio)Pharmaceuticals. *Bioconjug. Chem.* **2017**, *28*, 2372-2383.



A family of three picolinate pycnolone based ligands was studied for Tb<sup>3+</sup> and Lu<sup>3+</sup> coordination and radiolabeling with <sup>161</sup>Tb and <sup>177</sup>Lu in view of potential radiotherapeutic and theranostic radiotherapy/optical imaging applications.